Spectroscopic investigation of variations in the refractive index of a Nd:YAG laser crystal: Experiments and crystal-field calculations

J. Margerie, R. Moncorgé, and P. Nagtegaele
Centre Interdisciplinaire de Recherches Ions et Laser, UMR 6637 CNRS-CEA-ENSICAEN, Université de Caen, 6 Boulevard Maréchal Juin, 14050 Caen Cedex, France

(Received 25 July 2006; revised manuscript received 28 September 2006; published 13 December 2006)

The contribution of the $4f^3 \rightarrow 4f^2 5d$ interconfigurational optical transitions of Nd^{3+} which was supposed at the origin of the refractive index changes observed in the Nd:YAG laser crystal when it is pumped with high power laser diodes or flash lamps is investigated both theoretically and experimentally. Calculations based on crystal field determinations of energy levels and transition matrix elements as well as Kramers-Kronig relations confirm that these refractive index changes indeed come from variations of polarizabilities of the Nd^{3+} active ions when they are brought from their ground to their excited energy levels. The results indicate, however, that a supplementary contribution to such a purely dispersive effect could come from ligand to metal charge transfer transition.

DOI: 10.1103/PhysRevB.74.235108 PACS number(s): 78.20.Bh, 78.40.Ha, 78.55.Hx, 71.70.Ch

I. INTRODUCTION

It has long been known that a dynamical change of refractive index accompanies the optical excitation of laser active ions, such as Nd^{3+} and Cr^{3+} in a number of well known laser systems, because of the difference in polarizability of the ground and excited energy levels of these ions. The magnitude of this polarizability difference and the full understanding of the underlying mechanism, however, is still a matter of controversy or of skepticism. Indeed, a series of work have been dedicated these last years to that matter, more particularly in the case of Nd:YAG (Ref. 1) and Cr:LiSAF (Ref. 2), which prove that significant changes of refractive index and strong dependences of these changes on pump power and pump wavelength do occur. However, many researchers still neglect this process and, for example, base solely on absorption and gain saturation their description of dynamic nonlinear optical gratings, which are so promising for self-correction of laser beams in high power laser systems.

On the other hand, great efforts have been dedicated recently, from the experimental and theoretical standpoints, to the ground-state and excited-state UV absorption spectroscopy of a number of Ce^{3+}, Pr^{3+}, and Nd^{3+} doped fluoride crystals[3–6] in view of their potential as solid-state scintillators and/or broadband UV and VUV lasers. These works brought a large experience in the $4f^n \rightarrow 4f^{n-1}5d$ interconfigurational excited-state absorption processes of rareearth ions, which are so detrimental for laser operation of these laser systems. Since absorption and dispersion are intimately connected by Kramers-Kronig formulae, we were naturally led to extend our previous calculations[3–5] to examine the effect of the same $4f^n \rightarrow 4f^{n-1}5d$ transitions on the change of polarizability of the ions when they are brought into their metastable energy levels.

The present paper will concentrate on the case of Nd:YAG, because it is a very important material for high power laser systems and also because a number of experimental data are already available on $4f^3 \rightarrow 4f^2 5d$ ground state absorption (GSA) [Refs. 7–9], on $4f^3 \rightarrow 4f^2 5d$ excited state absorption (ESA) (Refs. 8, 10, and 11) and on polarizability differences between ground and metastable levels.[1,12,13] However, some of these experimental data are rather contradictory, as appears from a comparison of columns 2, 3, and 4 of Table I. Thus, they need to be checked by additional measurements. Moreover, Antipov *et al.*[1,13] report a very dramatic change of refractive index in the presence of IR+UV optical pumping, a fact which obviously calls for some experimental verification and more complete theoretical support.

The rest of the present paper will be divided into four parts. Section II will deal with an extension of previous calculations [made in the cases of $Pr:LiYF_4$ (Ref. 3), $Nd:LiYF_4$ (Ref. 4), and $Nd:BaY_2F_8$ (Ref. 5)] to derive the ESA spectra of Nd:YAG corresponding to the optical transitions to the $4f^2 5d$ band from the $^4F_{3/2}$ (11 427 cm^{-1}), $^2P_{3/2}$ (25 994 cm^{-1}), $^4D_{3/2}$ (27 571 cm^{-1}), and $^2F(2)_{5/2}$ (37 789 cm^{-1}) metastable levels[7,14] (see Fig. 1). The results corresponding to ESA transitions from the $^4F_{3/2}$ level will be confronted with ESA experimental data which have been carefully recorded and calibrated to give accurate peak positions and ESA cross sections. In Sec. III, the differences of polarizability between ground and metastable levels will be calculated for the above four metastable levels by applying the Kramers-Kronig transformation to the GSA and ESA spectra of Sec. II. The results of this calculation are compared in Sec. III B with the experimental data of Refs. 1 and 12. Section IV will be dedicated to the question of the very large polarizability change accompanying the population of the $^2F(2)_{5/2}$ level reported by Antipov *et al.*[1] In particular, we shall report the results of a three-beam experiment performed to validate some of the parameters used to describe the two-step excitation of this $^2F(2)_{5/2}$ metastable level. We shall finally discuss further, in Sec. V, the validity of our calculations and show that other processes, beside the one associated with the $4f^3 \rightarrow 4f^2 5d$ interconfigurational transitions, may also contribute to the polarizability differences between the ground and excited energy levels of Nd^{3+} in Nd:YAG.

TABLE I. $^4F_{3/2} \rightarrow 4f^2 5d$ absorption spectra (a) read on Fig. 1 (Ref. 8); (b) in the text of Ref. 10; (c) read on the dotted curve in Fig. 2 of Ref. 11.

	Experiment (Ref. 8)	Experiment (Ref. 10)	Experiment (Ref. 11)	Experiment (This work)	Theory (This work)
Position 1st max. (cm^{-1})	32800 (a)	33300 (b)	33500 (c)	32900	33000
Position 2nd max. (cm^{-1})	38000 (a)		39600 (c)	38800	38400
Intensity 1st max. (cm^2)		$2\ 10^{-18}$ (b)	$0.3\ 10^{-18}$ (c)	$0.8\ 10^{-18}$	$0.7\ 10^{-18}$
Intensity 2nd max. (cm^2)			$0.8\ 10^{-18}$ (c)	$1.9\ 10^{-18}$	$2.5\ 10^{-18}$
Intensity Ratio	0.7 (a)		2.5 (c)	2.35	3.4

II. $4f^3 \rightarrow 4f^2 5d$ GROUND- AND EXCITED-STATE ABSORPTION SPECTRA

A. Theoretical determination

The integrated absorption cross section around wave number $\upsilon_{i'i}$ corresponding to an electric-dipole allowed transition between states $|f^3, i'\rangle$ and $|f^2 d, i\rangle$ in a material with average refractive index n is given, for ρ polarized light, by (Refs. 3 and 15):

$$I^{\rho}_{i'i} = \int \sigma^{\rho}_{i'i}(\nu')d\nu' = \frac{2\pi^2}{h\varepsilon_0 c}\nu_{i'i}\frac{(n^2+2)^2}{9n}|\langle \Psi_{f^2d,i}|D_\rho|\Psi'_{f^3,i'}\rangle|^2, \tag{1}$$

where D_ρ is the ρ component of the electric dipole operator $\vec{D}$. The absorption cross section spectra at wave number υ, assuming Gaussian shape individual components with width δ at half maximum, are then given by (Refs. 3 and 15):

$$\sigma^{\rho}(\nu) = \sum_{i,i'} \frac{2}{\delta}\left(\frac{\ln 2}{\pi}\right)^{1/2} \varpi_{i'} I^{\rho}_{i'i} \exp\left[-\left(\frac{2\sqrt{\ln 2}(\nu-\nu_{i'i})}{\delta}\right)^2\right], \tag{2}$$

where $\varpi_{i'}$ is the relative Boltzmann equilibrium population of sublevel i'. To account for the isotropic distribution of the Y^{3+} substitutional sites in YAG, average is made over polarizations by writing:

$$\sigma(\nu) = \frac{\sigma^x(\nu)+\sigma^y(\nu)+\sigma^z(\nu)}{3}. \tag{3}$$

Absorption cross section spectra are thus built by determining the positions $\upsilon_{i'i}$ of the individual components, then by calculating the transition matrix elements $\langle \Psi_{f^2d,i}|D_\rho|\Psi'_{f^3,i'}\rangle$, which are obtained with the aid of the wave functions coming from the diagonalization of the Hamiltonian in the considered $4f^3$ and $4f^2 5d$ electronic configurations, and by adjusting the width δ to give the best fit to experimental band shapes.

These calculations have been made by using the Nd^{3+} free ion and crystal field parameters reported in Table II. Parameters $F^{(k)}(ff)$, α, β, γ, $T^{(k)}$, ζ_f, $M^{(k)}$, $P^{(k)}$, and $B_{kq}(f)$ used to describe the energy levels of the $4f^3$ ground-state configuration are those reported in Table I of Ref. 14. However, our $B_{kq}(f)$ parameters are those reported in Ref. 14 divided by a factor $(-)^l(2l+1)\binom{lkl}{000}$, with l=3, due a different definition of the B_{kq}s. Free ion and crystal field parameters $F^{(k)}(fd)$, $G^{(k)}\times(fd)$, ζ_d, and $B_{kq}(d)$ which describe the $4f^2 5d$ configuration are those already used in Refs. 4 and 5. The $B_{kq}(d)$ parameters are derived, as suggested in Ref. 5, by assuming $B_{2q}(d)=10.4\ B_{2q}(f)$ and $B_{4q}(d)=17.3\ B_{4q}(f)$.

The results are reported in Fig. 2 between 15 000 and 90 000 cm^{-1}. They are obtained by adjusting the position of the lowest sublevel of the $4f^2 5d$ excited configuration, noted A_1 in Table II and the width δ, as defined above, in order to give the best fit to the ground-state absorption data reported in Refs. 7–9. Figure 2(a) displays the ground- and first

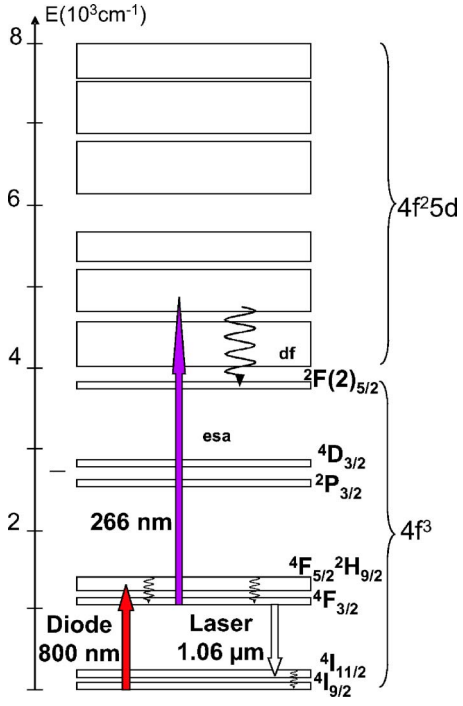

FIG. 1. (Color online) Energy levels of Nd^{3+} in $Y_3Al_5O_{12}$ (YAG).

TABLE II. Free ion and crystal field parameters used in the calculations (in cm^{-1}, except for $\langle r\rangle_{fd}$) (a) adjusted parameters; (b) parameters taken from [Ref. 14] and divided by a factor $(-)^l(2l+1)\begin{pmatrix} l & k & l \\ 0 & 0 & 0 \end{pmatrix}$ to account for a different definition of the B_{kq}'s; (c) parameters derived from the $B_{kq}(f)$ as explained in the text.

A_1	43300 (a)	T^4	39 [14]	P^2	275 [14]
F^2 (ff)	71090 [14]	T^6	−236 [14]	P^4	206.3 [14]
F^4 (ff)	50917 [14]	T^7	237 [14]	P^6	137.5 [14]
F^6 (ff)	34173 [14]	T^8	174 [14]	$B_{20}(f)$	505.0 (b)
F^2 (fd)	21221[4]			$B_{22}(f)$	115.6 (b)
F^4 (fd)	15927[4]	ζ_d	1077[4]	$B_{40}(f)$	−304.0 (b)
G^1 (fd)	9922[4]	$B_{20}(d)$	5252 (c)	$B_{42}(f)$	−2128.3 (b)
G^3 (fd)	11587[4]	$B_{22}(d)$	1202 (c)	$B_{44}(f)$	−969.7 (b)
G^5 (fd)	8300[4]	$B_{40}(d)$	−5259 (c)	$B_{60}(f)$	−1812.3 (b)
		$B_{42}(d)$	−36820 (c)	$B_{62}(f)$	−721.7 (b)
α	20.8 [14]	$B_{44}(d)$	−16776 (c)	$B_{64}(f)$	879.9 (b)
β	−651 [14]			$B_{66}(f)$	−654.6 (b)
γ	1868 [14]	ζ_f	875 [14]		
		M^0	2.58 [14]	$\langle r\rangle_{fd}$	0.245 Å [3]
T^2	231 [14]	M^2	1.44 [14]		
T^3	46 [14]	M^4	0.98 [14]	δ	2400 (a)

excited-state absorption bands $^4I_{9/2}\rightarrow 4f^25d$ and $^4F_{3/2}\rightarrow 4f^25d$, respectively. Figure 2(b) gathers those corresponding to the $^2P_{3/2}\rightarrow 4f^25d$, $^4D_{3/2}\rightarrow 4f^25d$, and $^2F(2)_{5/2}\rightarrow 4f^25d$ transitions.

According to Fig. 1 of Ref. 9 the onset of the GSA band is located around 40 800 cm^{-1}. This is in reasonable agreement with the energy mismatch of 2000 cm^{-1} reported in the same paper between the $^2F(2)_{7/2}$ level at 39 202 cm^{-1} (Ref. 14) and the onset of the GSA band. Since the position of the first electronic energy level of the $4f^25d$ configuration is taken as A_1=43 300 cm^{-1}, the energy difference (~2500 cm^{-1}) with the onset of the GSA band is simply due to vibronic effects. The first peak of the GSA band is located at 42 400 cm^{-1} (236 nm) in Ref. 9 and 44 700 cm^{-1} (224 nm) in Ref. 8. Our calculated value is 43 900 cm^{-1} (228 nm). According to Ref. 9, this absorption peak would correspond to an absorption coefficient of 3.87 cm^{-1}. Such a value, together with the sample Nd^{3+} ion density of 2×10^{20} cm^{-3}, means an absorption cross section of 1.9×10^{-20} cm^2, which seems unrealistic. The absorption cross section value of about 1 to 5 $\times10^{-18}$ cm^2 which is reported in Ref. 7, seems more reliable and, indeed, our theoretical calculations indicate a value of 3.6×10^{-18} cm^2. Thus, except for the absorption coefficient reported in Ref. 9, both our calculated position and cross section fit well to the experimental data so that the parameters of Table II may be used with some confidence as the basis of our further calculations.

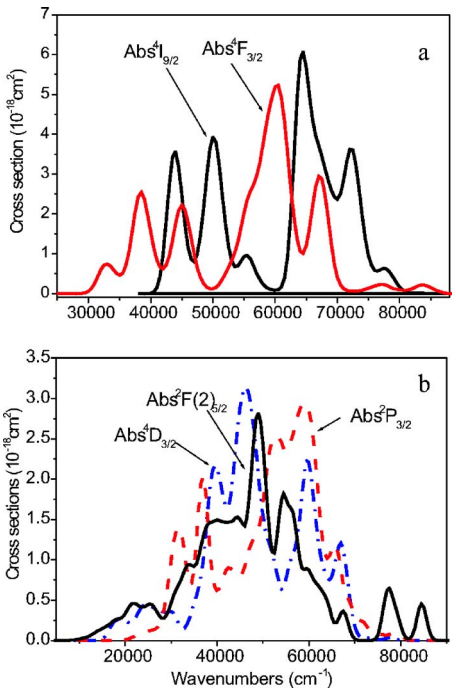

FIG. 2. (Color online) Calculated ground- and excited-state absorption cross section spectra (a) from levels $^4I_{9/2}$ and $^4F_{3/2}$, (b) from levels $^2P_{3/2}$, $^4D_{3/2}$, and $^2F(2)_{5/2}$.

Concerning ESA from the $^4F_{3/2}$ metastable level, more experimental data were necessary to further validate our calculations, since those reported in the literature[8,10,11] give contradictory results. In particular they do not agree concerning which is the more intense of the two lowest absorption peaks around 33 000 and 39 000 cm^{-1} [see Fig. 2(a)].

We thus performed an experiment which is detailed in the following subsection, not only for sake of clarity, but also to discuss some unexpected effects which have been observed in the course of these experiments and which might be related to our future discussion in Sec. V of increased refractive index changes in the presence of UV radiation

B. Excited-state absorption (ESA) measurements

These measurements were performed by using a pump-probe experimental setup which is schematically displayed in

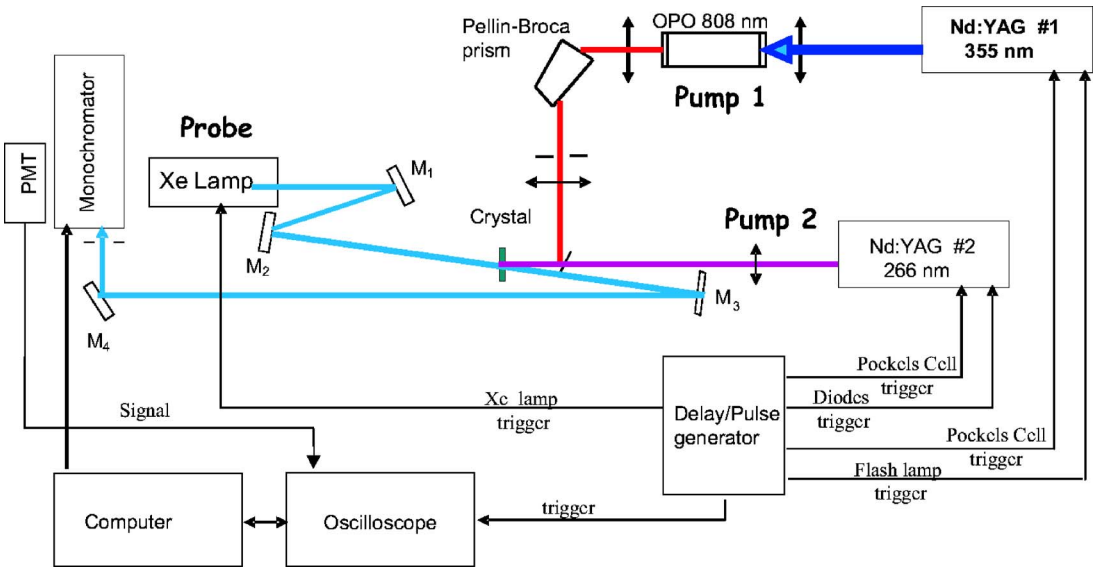

FIG. 3. (Color online) Setup for excited-state absorption (Sec. II B) and three-beams experiment (Sec. IV).

Fig. 3. The probe beam was provided either by a pulsed xenon-flash lamp with pulse duration of about 0.5 μs at half maximum or by a continuous-wave deuterium lamp. The pump beam was supplied by a 12 ns pulse Nd:YAG pumped OPO (Optical Parametric Oscillator) tuned at 808 nm, i.e., at the usual pump wavelength of Nd^{3+} corresponding to the ${}^4I_{9/2} \rightarrow {}^4F_{5/2}$ absorption transition. The probe beam was collimated and focused with the aid of curved mirrors to avoid chromatic dispersion effects and both probe and pump beams were propagating collinearly inside the crystal throughout a pinhole of 0.5 mm diameter. The crystal was a carefully characterized Nd:YAG sample of l=4.7 mm thickness containing 0.75 at % Nd, i.e., $N=1.035\times10^{20}$ ions/cm^3, giving rise to an absorption coefficient $\alpha \approx 4.5$ cm^{-1} at 808 nm.

In this kind of experiment, two transmission spectra are usually recorded, one (I_u) without the pump beam and the other (I_p) with both the probe and the pump beams. I_p and I_u are related by the following expressions:

$$I_u(\lambda) = I_0(\lambda)T^2(\lambda)\exp(-\sigma_{gsa}(\lambda)Nl), \quad (4)$$

$$I_p(\lambda) = I_0(\lambda)T^2(\lambda)\exp[-(\sigma_{gsa}(\lambda)N_g + \sigma_{esa}(\lambda)N_{ex})l], \quad (5)$$

where $T(\lambda)$ is the transmission of the air/crystal interface. Because of the fast ${}^4F_{5/2} \rightarrow {}^4F_{3/2}$ relaxation, we assume that the ${}^4I_{9/2}$ and ${}^4F_{3/2}$ ground- and excited-state populations, N_g and N_{ex}, respectively, are related to the total ion density N by $N_g+N_{ex}=N$. Then, the excited-state absorption cross-section σ_{esa} in the metastable level ${}^4F'_{32}$ can be determined by using the expression:

$$\sigma_{esa}(\lambda) = \sigma_{gsa}(\lambda) + \frac{1}{N_{ex}l}\ln\left(\frac{I_u}{I_p}\right). \quad (6)$$

Thus, such an ESA spectral determination not only requires the registration of clean and precise transmission spectra which means registrations of I_u and I_p spectra with stable light sources, at least during the time necessary for these registrations, but also a precise knowledge of the GSA spectrum in the considered wavelength domain. This might be particularly important in the case of Nd:YAG in the wavelength region around 265 nm where the ground-state absorption from ${}^4I_{9/2}$ to ${}^2F(2)_{5/2}$ overlaps with the excited state absorption from level ${}^4F_{3/2}$ to the $4f^25d$ excited configuration.

It is worth noting at this point, which has been known for a long time[16] but sometimes forgotten, that the GSA spectrum in this wavelength domain does not only consist of the sharp and tiny absorption lines associated with the UV levels ${}^2F(2)_{5/2}$ and ${}^2F(2)_{7/2}$ around 38 000 and 39 000 cm^{-1}, respectively. It also consists of a broad and rather intense absorption band which can be included (since it has nothing to do with some Nd^{3+} absorption) in the transmission term $T(\lambda)$ of the above expressions (4) and (5). This is the reason why we have reported the corresponding optical density spectrum (OD) of our Nd:YAG sample in the Fig. 4(a). It can be used, indeed, to estimate the order of magnitude of the GSA cross section appearing in expression (6), and to give an approximative value for this cross section at 266 nm, which will be very useful later on, in Sec. IV. According to expression (4), the OD is given by:

$$OD = \log\left(\frac{I_0}{I_u}\right) = \frac{\sigma_{gsa}Nl}{\ln 10} - 2\log T. \quad (7)$$

From this expression and the spectrum reported in Fig. 4(a), it is clear that the first term corresponding to Nd^{3+} absorption is much smaller than the second one. With $N=1.035\times10^{20}$ ions/cm^3 and l=4.7 mm, it means that the highest peak cross section around 262.5 nm does not exceed 1.9×10^{-21} cm^2.

The exact knowledge of the excited ion density N_{ex} is also a very crucial parameter. It is often evaluated by measuring the energy of the pump beam at the entrance and the output of the crystal. This method, however, may be tricky because it assumes that the probe and pump beams overlap very rigorously inside the entire crystal length which is rarely the

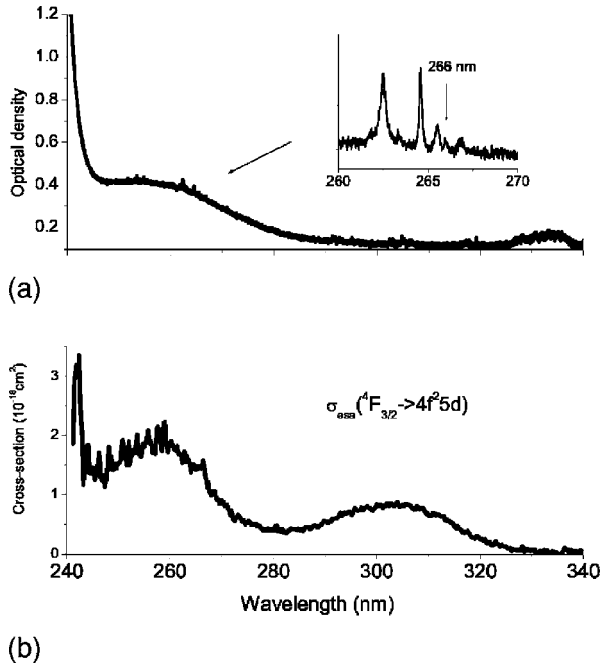

FIG. 4. Ground-state (a) and excited-state (b) absorption spectra registered in Nd:YAG by using a continuous wave deuterium lamp as probe beam.

case if one takes into account the exponential absorption profile of the pump beam inside the crystal. To improve the quality of this evaluation, it is thus recommended to proceed whenever possible with a complementary measurement by registering in the same experimental conditions, an excited state absorption spectrum in a wavelength region where the ground- and/or the excited-state absorption cross sections are more accurately known. This is what was performed here by recording pump/probe transmission spectra around 619 nm, a region corresponding to the relatively strong ($\sigma_{esa}=10.8\times10^{-20}$ cm^2) and well characterized[17] f-f excited-state absorption transition $^4F_{3/2}\rightarrow{}^4D_{3/2}$.

The resulting calibrated ESA spectrum recorded between 240 and 340 nm is reported in Fig. 4(b). According to this spectrum, the ground state absorption cross section σ_{gsa} with a maximum value of about 1.9×10^{-21} cm^2, is perfectly negligible compared to σ_{esa}. This was expected since the former and the latter correspond to ff and fd parity forbidden and parity allowed transitions, respectively. Our interconfigurational ESA experimental results are summarized in column 5 of Table I. They compare quite favorably with our Sec. II A calculations (column 6), as well as with the experimental intensity ratio of.Ref. 11. On the other hand, they completely discard the 0.7 intensity ratio of, Ref. 8 and the intensity of the first maximum as observed by Ref. 10 (too large) or by Ref. 11 (too small).

As mentioned above, we wish to report here some atypical behavior observed in the course of these measurements and which might be the reason why the ESA results reported in the past were so different from one another. As shown in Fig. 5, when use was made of a xenon flash lamp as probe beam, the ESA spectra around 250 nm were strongly perturbed with the appearance of sharp peaks corresponding to

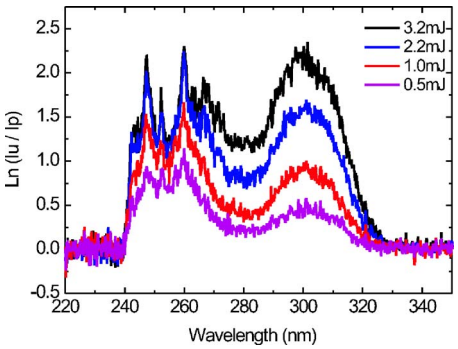

FIG. 5. (Color online) Excited state absorption spectra of Nd:YAG recorded by using a pulsed xenon lamp as probe beam versus pump energy at 808 nm.

increased transmission at particular wavelengths especially around 250 and 255 nm. Moreover, these perturbations were stronger and the relative intensity of the ESA band around 260 nm was lower as the excitation pump energy was higher. After having discarded some stimulated emission process since we do not know which emitting level would be responsible for it, as well as experimental artefacts, we believe that such observation might be assigned to some refractive index change, which will be analyzed in detail in the following section, leading to slightly different paths for the probe beam when the pump is on and off, an effect which would be more critical on the short wavelength side of our spectra due to the weak intensity of the probe beam in this wavelength domain but also, due to a stronger variation of refractive index in this wavelength domain.

III. THEORETICAL DERIVATION OF POPULATION-INDUCED POLARIZABILITY AND REFRACTIVE INDEX CHANGES

Polarizability and refractive index changes induced when the Nd^{3+} ions are brought into various metastable levels were calculated by using the Kramers-Kronig relations which allow one to connect variations of extinction coefficients (thus of absorption coefficients and absorption cross sections) and variations of refractive index (thus of polarizability).

A. Kramers-Kronig transformation

From the previously determined $\sigma_1(\nu)$ and $\sigma_2(\nu)$ spectra corresponding to the ground- and excited-state absorption bands to be considered, it is easy to derive the refractive index change $\Delta n(\nu)$ when N_{ex} ions are brought from their ground-state 1 into a particular excited-state 2 (see in Appendix A):

$$\Delta n(\nu) = n_2(\nu) - n_1(\nu), \tag{8}$$

with

$$n_i(\nu) = \frac{N_{ex}}{2\pi^2} P \int_0^\infty \frac{\sigma_i(\nu')}{(\nu'^2 - \nu^2)} d\nu', \tag{9}$$

where P stands for the Cauchy principal part of the integral.

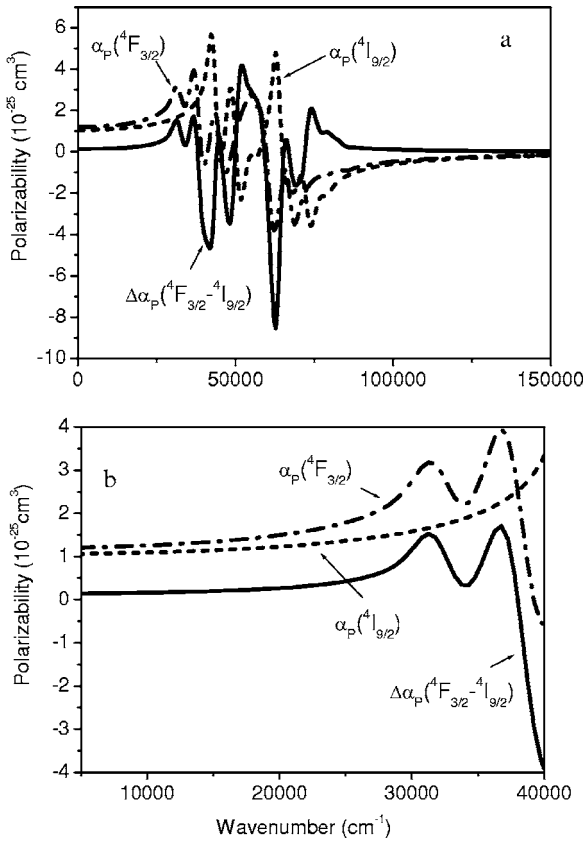

FIG. 6. Polarizability curves and polarizability change for levels $^4I_{9/2}$ and $^4F_{3/2}$ as found in Nd:YAG by using expressions (9) and (10) in the text.

The corresponding polarizability change $\Delta\alpha_p$ (noted Δp in Ref. 1) is then obtained by using formula (1) of this reference:

$$\Delta\alpha_p(\nu) = \frac{9n_0}{(n_0^2+2)^2} \times \frac{1}{2\pi} \times \frac{\Delta n(\nu)}{N_{ex}}, \qquad (10)$$

where n_0 is the refractive index at the considered wave number ν which will hereafter be kept constant with a value of 1.85, for sake of simplicity.

Figure 6(a) shows the polarizabilities $\alpha_{p1}(\nu)$ and $\alpha_{p2}(\nu)$ of

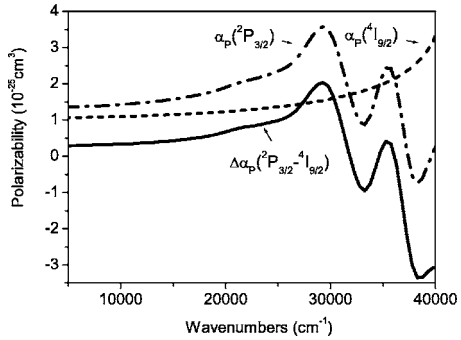

FIG. 7. Polarizability curves and polarizability change for levels $^4I_{9/2}$ and $^2P_{3/2}$ as found in Nd:YAG by using expressions (9) and (10) in the text.

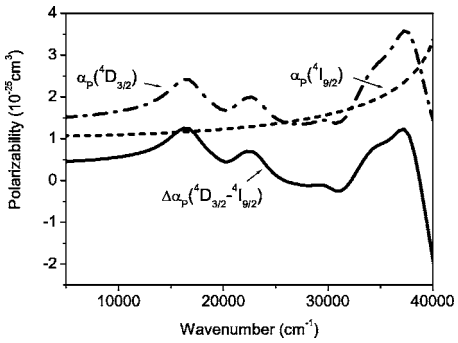

FIG. 8. Polarizability curves and polarizability change for levels $^4I_{9/2}$ and $^4D_{3/2}$ as found in Nd:YAG by using expressions (9) and (10) in the text.

levels $^4I_{9/2}$ and $^4F_{3/2}$ and their difference $\Delta\alpha_p = \alpha_{p2}(\nu) - \alpha_{p1}(\nu)$, as calculated at 295 K with the aid of formulae (8)–(10) and of the spectra reported in Fig. 2(a). Figure 6(b) is a zoom of these curves in the frequency domain 0–40 000 cm^{-1}. In fact, our calculated polarizability curves are expected to be physically significant only in the spectral region of YAG lattice transparency, i.e., for $\nu < 52\,000$ cm^{-1} (Ref. 7).

Figures 7–9 are similar to Fig. 6(b), except that the involved metastable states are $^2P_{3/2}$, $^4D_{3/2}$ and $^2F(2)_{5/2}$, respectively.

We also performed polarizability calculations, without explicit use of Kramers-Kronig transformation, in a model of damped harmonic oscillators (DHO). These alternative calculations have the advantage to allow direct comparison with those of previous authors[1,13] but they are less well founded than those using Eqs. (8)–(10), because the DHO model corresponds to Lorentzian absorption components (see in Appendix B), while experimental absorption line shapes are clearly Gaussian. However, the results of DHO calculations are found to be very close to Figs. 6(b) and 7–9 obtained by the Kramers-Kronig transformation. This arises from the fact that dispersion is a phenomenon with broad wings, in contradistinction to absorption. The spectral region of technical interest (i.e., 0-30 000 cm^{-1}) is sufficiently far from the region of intense $4f^3 \rightarrow 4f^2 5d$ transitions to yield a correct calculation of polarizability even from an approximate description of absorption. On the other hand, in the

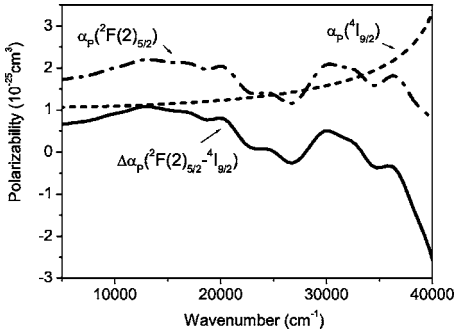

FIG. 9. Polarizability curves and polarizability change for levels $^4I_{9/2}$ and $^2F(2)_{5/2}$ as found in Nd:YAG by using expressions (9) and (10) in the text.

TABLE III. Observed and calculated polarizability differences.

Involved levels	Detection Wavelength (nm)	Observed $\Delta\alpha$ (cm^3) (Ref. 12)	Observed $\Delta\alpha$ (cm^3) (Ref. 12)	Calculated $\Delta\alpha$ (cm^3) (This Work)
$^4F_{3/2}-{}^4I_{9/2}$	514		$4.9\ 10^{-26}$	$2.6\ 10^{-2.6}$
$^4F_{3/2}-{}^4I_{9/2}$	633	$4.0\ 10^{-26}$		$2.1\ 10^{-26}$
$^2F(2)_{5/2}-{}^4I_{9/2}$	633	$100\ 10^{-26}$		$9.8\ 10^{-26}$

30 000–80 000 cm^{-1} domain, DHO calculations give quantitative results significantly different from those of Fig. 6(a), although they remain qualitatively similar.

B. Comparison with experimental data

We compare our results with the available experimental data in Table III. Our calculations give, for the metastable state $^4F_{3/2}$, $\Delta\alpha_{4F\text{-}4I}$ (514 nm) and $\Delta\alpha_{4F\text{-}4I}$ (633 nm) values approximately twice smaller than the experimental ones. A better agreement could be found just by multiplying the parameter $\langle r\rangle_{fd}$ of Table II by a factor of $\sqrt{2}$. This would also lead to a better agreement with the experimental ESA cross section of 2×10^{-18} cm^2 reported in Ref. 10 for level $^4F_{3/2}$ around 300 nm (see Table I). But this would spoil the good agreement between our own observed and calculated ESA cross sections and it would also increase the disagreement between our ESA calculated values and the observed values of Ref. 11.

If the polarizability discrepancies between our calculations and the experiments of Refs. 1 and 12 remain moderate in the case of the $^4F_{3/2}$ metastable state, they become very bad for the $^2F(2)_{5/2}$ level. Indeed, our theoretical calculations indicate a polarizability change $\Delta\alpha_{2F(2)\text{-}4I}$ (633 nm)=9.8×10^{-26} cm^3, ten times smaller than the experimental value.[1] *A priori*, three different causes may be at the origin of this discrepancy: (i) The experimental value may be overestimated. (ii) We may have badly calculated the contribution of the $4f^3\rightarrow4f^25d$ interaction to the polarizability differences. (iii) Other transitions, beside $4f^3\rightarrow4f^25d$, may contribute heavily to these polarizability differences. Sections IV and V are dedicated respectively, to the analysis of these three hypotheses.

IV. POLARIZABILITY CHANGE IN THE $^4I_{9/2}\rightarrow{}^2F(2)_{5/2}$ TRANSITION

The polarizability change $\Delta\alpha_{2F(2)\text{-}4I}$ (633 nm) $\approx10^{-24}$ cm^3 reported in Ref. 1 was deduced from the refractive index change observed under the combined effect of pumping around 808 and 266 nm. Pumping around 808 nm leads to population of level $^4F_{3/2}$ whereas pumping around 266 nm leads to population of level $^2F(2)_{5/2}$ either directly, but, as mentioned above, with a very low absorption cross section, or, more efficiently, via a two-step process: absorption from metastable $^4F_{3/2}$ up into the $4f^25d$ excited configuration followed by a rapid radiationless relaxation down to the upper $4f^3$ levels, among which the long lived $^2F(2)_{5/2}$ emitting level.

In this hypothesis, the observed refractive index change can be described, according to relation (10), by the expression:

$$\Delta n(\nu)=\frac{2\pi(n_0^2+2)^2}{9n_0}(N_{4F3/2}\Delta\alpha_{4F-4I}(\nu)+N_{2F(2)5/2}\Delta\alpha_{2\ F(2)-4I)}(\nu)), \tag{11}$$

where $N_{5F3/2}$ and $N_{2F(2)5/2}$ are the populations of the $^4F_{3/2}$ and $^2F(2)_{5/2}$ levels, $\Delta\alpha_{4F\text{-}4I}$ and $\Delta\alpha_{2F(2)\text{-}4I}$ the associated polarizability changes with respect to the ground-state $^4I_{9/2}$. Assuming, in their experimental conditions, that only a small fraction ε of the Nd^{3+} ions transits from the $^4F_{3/2}$ level to the $^2F(2)_{5/2}$ level, the authors of Ref. 1 found that the product $\varepsilon\Delta\alpha_{2F(2)\text{-}4I}$ should be equal to about 1.5×10^{-26} cm^3 at 633 nm. Introducing the energy density W_p^{266} (noted W_{4h} in Ref. 1), the ESA cross section σ_{esa}^{266} and the energy of the pump photons $h\nu_{266}$ (noted $h\nu_{4h}$ in Ref. 1) at 266 nm as well as the quantum efficiency β_{df} describing the part of the absorbed pump photons which is used to populate the $^2F(2)_{5/2}$ level via the $4f^25d$ excited configuration, and using the approximate relation:

$$\varepsilon=\frac{N_{2F(2)5/2}}{N_{4F3/2}}\approx\beta_{df}\frac{\sigma_{esa}W_p^{266}}{h\nu_{266}} \tag{12}$$

the authors derived the value $\varepsilon\approx0.015$, by taking $W_p^{266}\approx0.05$ J/cm^2, $\sigma_{esa}^{266}\approx7\times10^{-19}$ cm^2 and $\beta_{df}\approx0.3$. However, if one takes $\beta_{df}\approx0.7$, which will be justified in Sec. IV B and $\sigma_{esa}^{266}\approx1.5\times10^{-18}$ cm^2, which is our experimental value, one obtains $\varepsilon\approx0.07$. Then, the experimental value for $\Delta\alpha_{2F(2)\text{-}4I}$ would be equal to 2.1×10^{-25} cm^3, much closer to our theoretical value of 9.8×10^{-26} cm^3 derived in Sec. III. In this hypothesis, our calculated values of Table III would be underestimated by similar factors 0.53, 0.52 and 0.46 for $\Delta\alpha_{4F\text{-}4I}$ (514 nm), $\Delta\alpha_{4F\text{-}4I}$ (633 nm) and $\Delta\alpha_{2F(2)\text{-}4I}$ (633 nm) respectively.

We obtained the above introduced value $\beta_{df}\approx0.7$ by performing the three-beams experiment schematically shown in Fig. 3. The crystal transmission was probed by a xenon flash lamp while it is pumped around 808 nm with a *Q*-switched (10 ns pulse duration) Nd:YAG pumped OPO from Spectron. The 0.5 μs xenon pulse was switched on around 10 μs after the laser pulse and the probe light integrated over 2 μs. The resulting ESA spectra recorded around 300 nm thus could be used through expression (6) to control the effective excited ion density $N_{ex}=N_{4F3/2}$. The setup was also used, however, to record, as in (Ref. 18), the fluorescence spectrum resulting from the excitation of the higher lying metastable state

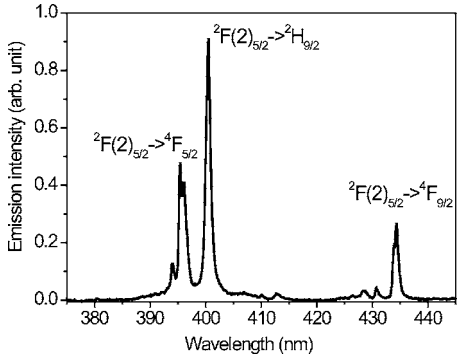

FIG. 10. Emission spectrum of Nd:YAG recorded after 266 nm or 808+266 nm excitation.

$^2F(2)_{5/2}$. This was performed by exciting this level either directly around 266 nm, with the aid of a second (10 ns pulse duration, frequency-quadrupled) Nd:YAG pulsed laser (Diva model from Thales-Laser) synchronized with the former, or both directly and indirectly, via the excited-state absorption followed by the relaxation process: $^4F_{3/2} \rightarrow 4f^2 5d \rightarrow {}^2F(2)_{5/2}$ (see Fig. 1). The 266 nm laser pulse was switched on about 7.5 μs after the 808 nm one and the time-resolved fluorescence spectra, as the ESA spectra, could be recorded between 10 and 12 μs after the 808 nm pulse. Knowing that the emission lifetimes of the $^4F_{3/2}$ and $^2F(2)_{5/2}$ levels are equal to about 250 and 3.1 μs, that the lifetimes of the other emitting states $^4G_{7/2}$, $^2P_{3/2}$, and $^4D_{3/2}$ are much shorter, with values of 0.37, 300, and 2.2 ns, respectively,[19] and that the $4f^2 5d \rightarrow {}^2F(2)_{5/2}$ relaxation process occurs likely within less than a few nanoseconds, the fluorescence spectra recorded between about 320 and 450 nm (see in Fig. 10) could be assigned to emission transitions from level $^2F(2)_{5/2}$ without any ambiguity. It also means that when the 266 nm pulses arrive onto the system, more than 95% of the ions which have been excited with the 808 nm photons still remain in the $^4F_{3/2}$ metastable level. The aim of the experiment was thus to follow the intensity of one of the $^2F(2)_{5/2}$ emission lines as a function of the 266 nm pulse energy, knowing the real $^4F_{3/2}$ excited ion density, and to compare the intensity of these emission lines in the absence and the presence of pumping of the $^4F_{3/2}$ level around 808 nm.

Assuming, as in Ref. 1, that the only excitation processes which can be considered, consist in a direct excitation of the $^2F(2)_{5/2}$ emitting level, in case of 266 nm pump photons, and in a two-step excitation via the $^4F_{3/2}$ metastable level and the $4f^2 5d$ excited electronic configuration, in case of simultaneous pumping around 808 and 266 nm, the intensity of the collected emission lines should be approximately proportional to the $^4I_{9/2}$ and $^4F_{3/2}$ ion densities according to the expressions,

$$I_{2F5/2} = aN_{2F5/2} \approx a\frac{\sigma_{gsa}^{266} W_p^{266}}{h\upsilon_{266}} N_T \tag{13}$$

in case of direct excitation at 266 nm, N_T standing for the total Nd^{3+} ion density in the crystal, and

$$I'_{2F5/2} = aN'_{2F5/2} \approx a\beta_{df}\frac{\sigma_{esa}^{266} W_p^{266}}{h\upsilon_{266}} N_{4F3/2} \tag{14}$$

in case of two-step excitation at 808 and 266 nm.

Consequently, provided that the involved cross sections are known with enough accuracy and the effective excited ion density $N_{4F3/2}$ can be determined *in situ*, the ratio of these intensities should give a good estimate of β_{df} by writing:

$$\beta_{df} = \frac{I'_{2F(2)5/2}}{I_{2F(2)5/2}} \frac{\sigma_{gsa}^{266}}{\sigma_{esa}^{266}} \frac{N_T}{N_{4F3/2}}. \tag{15}$$

With a crystal containing 0.75% Nd, thus 1.035×10^{20} Nd ions/cm^3, an effective excited ion density $N_{4F3/2} \approx 1.6 \times 10^{18}$ cm^{-3} and excitation laser pulses at 266 nm of about 0.035 J/cm^2 (which does not come into play in the calculations), we obtained an intensity increase measured on the lines located around 400 and 440 nm by a factor of 62, in nice agreement with the factor of 50 observed by the authors of Ref. 18, whose experimental conditions slightly differ from ours. Using our experimental values, i.e., $\sigma_{esa}^{266} \approx 1.5 \times 10^{-18}$ cm^2 and $\sigma_{gsa}^{266} \approx 2.5 \times 10^{-22}$ cm^2 [value derived from the spectrum of Fig. 4(a)] we get from formula (15), $\beta_{df} \approx 0.7$.

V. DISCUSSION

A. Did we calculate reliably the $4f^3 \rightarrow 4f^2 5d$ contribution to polarizability changes ?

Two parameters A_1 and δ (Table II) were adjusted to fit GSA experimental data. Our choice may have been unlucky. Therefore: We modify the energy mismatch (parameter A_1) between the ground and excited configurations in the 41 300–45 300 cm^{-1} domain, which is well beyond its possible values in view of available experimental results concerning the onset of $4f^3\ {}^4I_{9/2} \rightarrow 4f^2 5d$ transitions. It is found that, for this range of A_1 values, $\Delta\alpha_{4F\text{-}4I}$ (633 nm) varies from 2.35 to 1.82×10^{-26} cm^3 and $\Delta\alpha_{2F(2)\text{-}4I}$ (633 nm) from 8.69 to 10.41×10^{-26} cm^3. Thus, uncertainty about the exact value of A_1 cannot account for the large discrepancy between observed and calculated values of $\Delta\alpha_{2F(2)\text{-}4I}$.

We modify the width δ introduced to "dress" the individual components of the various absorption spectra. A reduction of the chosen value of 2400 cm^{-1} could contribute to an increase of the absorption peak cross sections and of the resulting polarizability changes. However, taking $\delta = 1200$ cm^{-1}, it is found that $\Delta\alpha_{2F(2)\text{-}4I}$ (633 nm) only increases by 0.6%, which is far from being enough.

In pulsed operation, there might exist a large local temperature rise which would make the relative populations $\varpi_{i'}$ of the various sublevels of the ground- and metastable-states to be very different from Boltzmann equilibrium. *Via* formulae (2) and (9), this would introduce a refraction index variation of thermal origin, but with a characteristic time constant equal to the lifetime of the metastable level. Such an effect is simulated by introducing into the calculation a temperature of 600 K (instead of room temperature), either for calculating the $\varpi_{i'}$'s of the metastable state, or the $\varpi_{i'}$'s of both

ground and metastable states. In both hypotheses, the effect on calculated $\Delta\alpha'$s is found to be less than 1.3%.

If we replace the Kramers-Kronig calculation by the use of a damped harmonic oscillator model (end of Sec. III A), it lowers $\Delta\alpha_{2F(2)-4I}$ from 9.8 to 8.6 10^{-26} cm^3, a rather small change, and moreover in the "wrong" direction.

B. Other contribution(s) to polarizability changes ?

From our different unsuccessful endeavors of Sec. V A, it appears that our calculation of Sec. III A is probably intrinsically reliable. But its frame may be too restricted. Beside $4f^3 \rightarrow 4f^2 5d$, other transitions probably contribute quite significantly to the polarizability changes observed when Nd^{3+} ions are brought from $^4I_{9/2}$ to some metastable level. We shall consider below two possibilities, without claiming that they are the only ones.

1. $4f^3 \rightarrow 4f^3$ transitions

They are parity forbidden and therefore much weaker than the $4f^3 \rightarrow 4f^2 5d$ transitions, so that their effect is negligible "on the far wings," i.e., at large spectral distances. But in the immediate vicinity of a $4f^3 \rightarrow 4f^3$ line, one may expect a very sizeable "resonant" effect. This was considered in detail by Antipov *et al.*[1] for $\Delta\alpha_{4F-4I}$ in the 9300–9600 cm^{-1} domain, i.e., in the spectral region of $^4F_{3/2} \rightarrow {}^4I_{11/2}$ transitions. In the present case of $\Delta\alpha_{2F(2)-4I}$, we can expect similar resonant effects if some stimulated emission of level $^2F(2)_{5/2}$ would coincide with the probe light used in the experiments. Knowing that level $^2F(2)_{5/2}$ lies at 37 789 cm^{-1} (Ref. 14) and that the probe light of Ref. 1 was that of an He-Ne laser at 632.82 nm (15 802 cm^{-1}), this stimulated emission should occur toward a sublevel near 37 789−15 802=21 987 cm^{-1}. According to (Ref. 14), this wave number corresponds to the group of levels $^2G(1)_{9/2}$, $^2D(1)_{3/2}$, $^4G_{11/2}$, $^2K_{15/2}$. More precisely, it is close to the positions of the 96th and 97th sublevels of the $4f^3$ configuration observed at 21 906 and 22 036 cm^{-1}, respectively. The question is to know whether the optical transitions from $^2F(2)_{5/2}$ to these sublevels are sufficiently strong. The experimental signature of such a resonant effect would be a great sensitivity of the observed $\Delta\alpha_{2F(2)-4I}$ (λ) to the analysis wavelength.

A resonant effect would also be expected if a $4f^3 \rightarrow 4f^3$ absorption of $^2F(2)_{5/2}$ did coincide with the probe light wave number. But such is not the case since 37 789+15 802 =53 591 cm^{-1} which, according to our calculations of Sec. II A, falls very far both from the expected positions of the 175th and 176th sublevels of configuration $4f^3$ (48 354 and 64 626 cm^{-1}, respectively).

2. Charge transfer bands

Charge transfer bands are intense and situated in the VUV; they should contribute significantly to the polarizability of Nd^{3+} ions, both in its ground and in its metastable levels. The chief problem is that nothing is precisely known about charge transfer bands in Nd:YAG (they are concealed under the fundamental absorption of YAG matrix). For lack of a better hypothesis, we shall assume that charge transfer from $^4I_{9/2}$, $^4F_{3/2}$ or $^2F(2)_{5/2}$ may be represented by a single transition toward the same excited level, with a Gaussian line shape and with the same oscillator strength and the same spectral width in the three cases.

From Ref. 20 the charge transfer band in Yb:YAG is 6000 cm^{-1} broad and is centerd at 47 600 cm^{-1}. Let us add to this position the difference in ionization energies[21] of free Yb^{2+} and Nd^{2+} ions 202 070−178 600=23 470 cm^{-1}. We thus obtain an estimate of 47 600+23 470$\sim$71 000 cm^{-1} for the GSA transfer band in Nd:YAG. Keeping the 6000 cm^{-1} breadth and assuming an oscillator strength f=0.029, the contribution of charge transfer to polarizability at 632.82 nm would be (in 10^{-26} cm^3) 4.34, 6.31, and 25.09 for $^4I_{9/2}$, $^4F_{3/2}$, and $^2F(2)_{5/2}$, respectively. Adding this contribution to the one of $4f^3 \rightarrow 4f^2 5d$, one obtains:

$$\Delta\alpha_{4F-4I} = [2.05 + (6.31 - 4.34)]10^{-26}\ \text{cm}^3 = 4.0\ 10^{-26}\ \text{cm}^3,$$

$$\Delta\alpha_{2F(2)-4I} = [9.75 + (25.09 - 4.34)]10^{-26}\ \text{cm}^3$$
$$= 30.5\ 10^{-26}\ \text{cm}^3.$$

The first value exactly agrees with the experimental $\Delta\alpha_{4F-4I}$(633 nm), which is hardly surprising since the value of f was precisely adjusted to secure this result! The second value may be considered as compatible with the experimental result of Ref. 1, if one takes into account our value (1.5 $\times 10^{-18}$ cm^2) of σ_{esa}^{266} and considers the uncertainty about the exact value of the quantum efficiency β_{df} (see Sec. IV A).

In the end, it is clear that such an interesting hypothesis now remains to be proved by evaluating the strength of the considered charge-transfer bands, either experimentally or theoretically, which may be difficult in a short term. An evaluation of this possible contribution can be reached, however, more indirectly, by investigating the case of Yb:YAG, another very important laser material for which large refractive index variations have been recently evidenced[23] and for which, unlike Nd:YAG, the onset of the lowest ligand to metal charge transfer band, as mentioned above, has been proved[20] to be located around 220 nm, thus below the interconfigurational f-d bands of the Yb^{3+} ions.

VI. CONCLUSION

The refractive index variations which have been recently observed in the case of Nd:YAG following diode laser, flashlamp or diode+UV laser excitation have been reconsidered and analyzed both theoretically and experimentally. It is now definitely confirmed that dispersive effects coming from variations of polarizability of the Nd^{3+} ions when they are brought from their ground to their successive excited energy levels play a major role. These variations of polarizability are primarily due to the proximity of the very intense (electric-dipole allowed) absorption bands associated with the lowest energy levels of the first excited electronic configuration $4f^2 5d$. It is noted however, that some supplementary dispersive effect should also contribute and that ligand to metal charge transfer bands could be at the origin of this supplementary contribution.

To conclude, it is worth noting that with Nd^{3+}, the ligand to metal charge transfer bands cannot be observed and analy-

sed since the corresponding transitions always lie at higher energies than the $4f^3-4f^25d$ interconfigurational ones. In the case of Yb^{3+}, however, and more particularly in the case of Yb:YAG, another high power laser system, it is known that charge transfer bands lie at lower energies and that large refractive index variations can be observed. Thus, works are now in progress with Yb^{3+} doped systems to analyse and estimate the contribution of this type of charge transfer bands to the variation of polarizability of the Yb^{3+} ions when they are brought from their ground to excited energy levels.

ACKNOWLEDGMENTS

Part of this work has been performed within the framework of an INTAS collaborative program No. 03-4893 dedicated to "Next generation lasers using self-organized dynamic holographic cavities." Thanks are expressed to O. Antipov from the Institute of Applied Physics (Nizhny-Novgorod, Russia) for fruitful discussions and to J.P. Huignard (Thales) for his interest in this work.

APPENDIX A

According to Eq. (18.1) of Ref. 22:

$$n(\omega)-1=\frac{2}{\pi}P\int_0^\infty \frac{\omega'\kappa(\omega')}{(\omega'^2-\omega^2)}d\omega', \tag{A1}$$

where $n(\omega)$ stands for the refractive index, ω, and ω' for pulsations, and where the extinction coefficient (is related to the absorption k by:

$$k(\omega)=\frac{4\pi\kappa(\omega)}{\lambda}=4\pi\nu\kappa(\omega). \tag{A2}$$

Using wave numbers ν instead of pulsations, thus writing $\nu\prime=\frac{\omega\prime}{2\pi c}$, (A1) becomes:

$$n(\nu)-1=\frac{2}{\pi}P\int_0^\infty \frac{\nu'\kappa(\nu')}{(\nu'^2-\nu^2)}d\nu'=\frac{1}{2\pi^2}P\int_0^\infty \frac{k(\nu')}{(\nu'^2-\nu^2)}d\nu'. \tag{A3}$$

Writing $n_i(\nu)$ for the part of the refractive index arising from the Nd^{3+} ions in the state i and using $k_i=\sigma_i N_{ex}$, where N_{ex} is the relevant density of Nd^{3+} ions, the above expression yields Eq. (9) of the main text.

APPENDIX B

Starting with the usual expression for the polarizability α_P obtained on the basis of the classical oscillator model and using for example the formula (2) of Ref. 13 expressed in our case as a function of wavenumbers ν one obtains after separation of the real and imaginary parts:

$$\alpha_P(\nu)=\frac{q^2}{16\pi^3\varepsilon_0 mc^2}\sum_i \frac{f_{i\prime,i}(\nu'^2-\nu^2)}{[(\nu'^2-\nu^2)^2+\nu^2\delta^2]}. \tag{B1}$$

This expression gives the polarizability of the ion in a level $i\prime$ at the wave number ν as determined by all the possible transitions of wave number $\nu\prime$ to levels i characterized by the oscillator strengths $f_{i\prime,i}$ given, in our case, by:

$$f_{i\prime,i}=\frac{8\pi^2 m\nu' c}{hq^2}\times\frac{|\langle\Psi_{f^2d,i}|\vec{D}|\Psi'_{f^3,i\prime}\rangle|^2}{3} \tag{B2}$$

in which q and m are the charge and mass of the electron, respectively, and the $\langle\Psi_{f^2d,i}|\vec{D}|\Psi\prime_{f^3,i\prime}\rangle$ are the transition matrix elements which have been determined in Sec. II.

Inserting (B2) into (B1) and averaging over the relative populations $\bar{\omega}_i$' of the sublevels of the starting configuration $4f^3$, one obtains:

$$\alpha_P(\nu)=\frac{1}{2\pi h\varepsilon_0 c}\sum_{i,i'}\frac{\nu'(\nu'^2-\nu^2)}{[(\nu'^2-\nu^2)^2+\nu^2\delta^2]}\times\frac{|\langle\Psi_{f^2d,i}|\vec{D}|\Psi'_{f^3,i'}\rangle|^2}{3}\varpi_{i'} \tag{B3}$$

an expression which can used successively to estimate the polarizability in the considered ground and metastable excited states $^4I_{9/2}$, $^4F_{3/2}$, $^2P_{3/2}$, $^4D_{3/2}$, and $^2F(2)_{5/2}$, respectively, then to derive the associated polarizability changes.

It is worth noting here that writing (B2) and (B3), choice has been made implicitly to "dress" the components of the underlying absorption spectra with Lorentzian curves of width δ, which is not the choice made (Gaussian shape components), in the beginning, in our analysis of the spectra. In fact, the above expression (B3) only leads to Lorentzian shape components in the limit of narrow linewidths δ. For broad linewidths, the shape of the components will be quasi-Lorentzian and should not differ very much from Gaussians.

[1] O. L. Antipov, O. N. Eremeykin, A. P. Savikin, V. A. Vorob'ev, D. V. Bredikhin, and M. S. Kuznetsov, IEEE J. Quantum Electron. **39**, 910 (2003) and references therein.
[2] N. Passilly, M. Fromager, K. Ait-Ameur, R. Moncorgé, J. L. Doualan, A. Hirth, and G. Quarles, J. Opt. Soc. Am. B **21**, 531 (2004).
[3] M. Laroche, J. L. Doualan, S. Girard, J. Margerie, and R. Moncorgé, J. Opt. Soc. Am. B **17**, 1291 (2000).
[4] A. Collombet, Y. Guyot, M. F. Joubert, M. Laroche, J. Margerie, R. Moncorgé, and E. Descroix, Phys. Rev. B **68**, 035115 (2003).
[5] A. Collombet, Y. Guyot, M. F. Joubert, J. Margerie, R. Moncorgé, and A. Tkachuk, J. Opt. Soc. Am. B **21**, 2053 (2004).
[6] M. F. Reid, L. van Pieterson, R. T. Wegh, and A. Meijerink, Phys. Rev. B **62**, 14744 (2000).
[7] M. J. Weber, Solid State Commun. **12**, 741 (1973).
[8] N. Yu. Konstantinov, L. G. Karaseva, V. V. Gromov, and A. V. Yakovlev, Phys. Status Solidi A **83**, K153 (1984).
[9] S. K. Gayen and B. Q. Xie, J. Opt. Soc. Am. B **10**, 993 (1993).

[10] M. A. Dubinskii and A. L. Stolov, Sov. Phys. Solid State **27**, 1315 (1985).
[11] Y. Guyot, S. Guy, and M. F. Joubert, J. Alloys Compd. **323-324**, 722 (2001).
[12] R. C. Powell, S. A. Payne, L. L. Chase, and G. D. Wilke, Opt. Lett. **14**, 1204 (1989).
[13] O. L. Antipov, A. S. Kuzhelev, D. V. Chausov, and A. P. Zinov'ev, J. Opt. Soc. Am. B **16**, 1072 (1999).
[14] J. B. Gruber, M. E. Hills, T. H. Allik, C. K. Jayasankar, J. R. Quagliano, and F. S. Richardson, Phys. Rev. B **41**, 7999 (1990).
[15] B. Di Bartolo, in *Optical Interactions in Solids* (John Wiley and Sons, Inc., New York, 1968), for example.
[16] M. A. Kramer and R. W. Boyd, Phys. Rev. B **23**, 986 (1981).
[17] Y. Guyot, H. Manaa, J. Y. Rivoire, R. Moncorgé, N. Garnier, E. Descroix, M. Bon, and P. Laporte, Phys. Rev. B **51**, 784 (1995).
[18] O. L. Antipov, O. N. Eremeikin, and A. P. Savikin, Quantum Electron. **32**, 793 (2002).
[19] T. T. Basiev, A. Yu. Dergachev, and Yu. V. Orlovski, Trudy IOF RAN **46**, 3 (1994).
[20] L. Van Pieterson, Ph.D. thesis, Utrecht, 2001.
[21] W. C. Martin, R. Zalubas, and L. Hagen, *Atomic Energy Levels. The rare earth elements* (National Bureau of Standards, Washington, D.C., 1978).
[22] F. Stern, Solid State Phys. **15**, 299 (1963).
[23] O. L. Antipov, D. V. Bredikhin, O. N. Eremeykin, A. P. Savikin, E. V. Ivakin, and A. V. Sukhadolau, Opt. Lett. **31**(6), 763 (2006).